

Scenarios for physics experiments in the COMPASS Upgrade tokamak

F. Jaulmes¹, M. Komm¹, O. Grover^{1,2}, J. Seidl¹, P. Snyder³, O. Shyshkin¹, M. Imrisek¹,
G. Zadvistkiy¹, J. Gerardin¹, I Borodkina¹, R. Dejarnac¹, D. Tskhakaya¹, V. Weinzettl¹,
M. Peterka¹, M. Hron¹, R. Panek¹, and the COMPASS team¹

¹ IPP of the Czech Academy of Science, Za Slovankou 3, CZ-182 00 Prague, Czech Republic

² Max-Planck-Institut für Plasmaphysik, Boltzmannstr. 2, 85748 Garching, Germany

³ General Atomics, San Diego, CA 92186-5608, United States of America

Introduction

The COMPASS Upgrade tokamak [1] will have dimensions $R_0=0.894\text{m}$ and $a\approx 0.275\text{m}$ with high-field ($B_t\approx 5\text{T}$), high-current ($I_p\approx 2\text{MA}$), high-triangularity ($\delta\approx 0.5$) capabilities. The machine will build on and expand upon the scientific results of Alcator C-Mod [2].

Various scenarios of Edge Transport Barriers

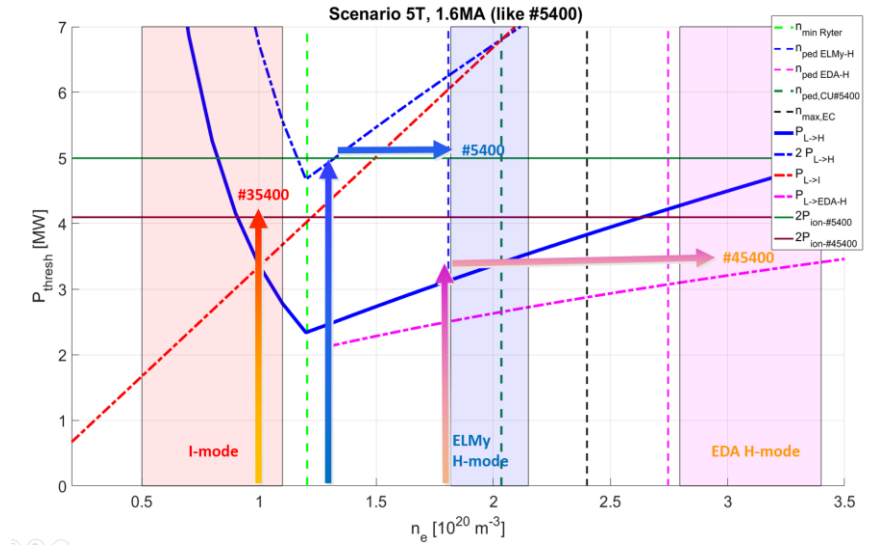
ELMy H-mode is best accessed at the minimum power at the density $n_{e,\text{min,Ryter}}$ [3] and the threshold in heating power to enter ELMy H-mode is given in [4]. At higher magnetic field and plasma triangularity, we anticipate accessibility to three distinct ETBs: ELMy H-mode [4,5], Enhanced D-Alpha (EDA) H-mode [6,7] and I-mode [8].

	Threshold power [MW]	$n_{\text{ped}} [10^{20}\text{m}^{-3}]$	$\tau_E [s]$
ELMy H-mode	$P > P_{L\rightarrow H}, n_e > n_{e,\text{min}}$	$\simeq 2.5B_{\text{pol}}$	$\tau_{H98(y,2)}$
I-mode	$0.162n_{e,20}B_t^{0.26}S$	no pedestal	$\sim 0.8\tau_{H98(y,2)}$
EDA H-mode	$0.054n_{e,20}^{0.49}B_t^{0.85}S^{0.84}$	$3.57I_p^{0.52}n_{e,L}^{0.52}B_t^{-0.38}$	$\tau_{H98(y,2)}$

Detailed integrated transport modelling with the METIS code [9] yields density and temperature profiles during the flat-top. The table below summarizes the plasma parameters of the main COMPASS Upgrade physics scenarios: the ELMy H-mode pedestals are #24300 and #5400, I-modes #35300 and #35400, EDA H-modes #44310 and #45400.

Scenario	B_t [T]	I_p [MA]	q_{95}	n_e [10^{20}m^{-3}]	$P_{\text{NBI}+\text{P}_{\text{EC}}}$ [MW]	P_{sep} [MW]	$n_{e,\text{ped}}$ [10^{20}m^{-3}]	$T_{e,\text{ped}}$ [eV]	v_{ped}^*
#24300	4.3	1.2	4.1	1.9	3+1	2.8	1.78	928	0.95
#5400	4.9	1.6	3.5	2	4+2	3.8	1.97	1361	0.47
#35300	4.9	1.6	3.4	1	3+1	4.2	0.49	2467	0.09
#35400	5	1.6	3.5	1	4+2	5	0.46	2136	0.11
#44310	4.3	1.2	4.2	3	3+0	1.1	2.7	597	2.52
#45400	5	1.6	3.6	3	4+0	2.2	2.87	908	0.93

According to C-Mod results, the type of ETB is strongly dependent on the density at which the main external heating is switched on. The density will then increase at the pedestal top to match the value given by the scaling in the table.



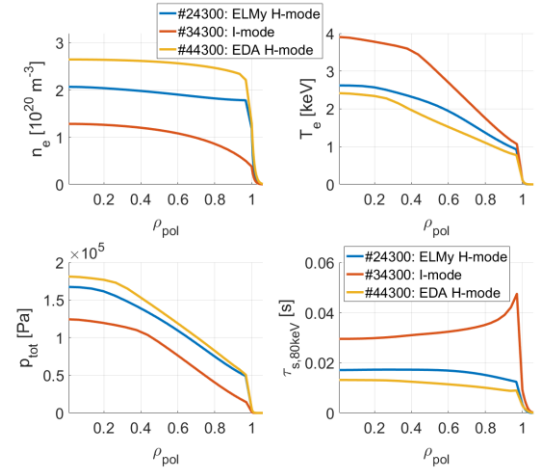
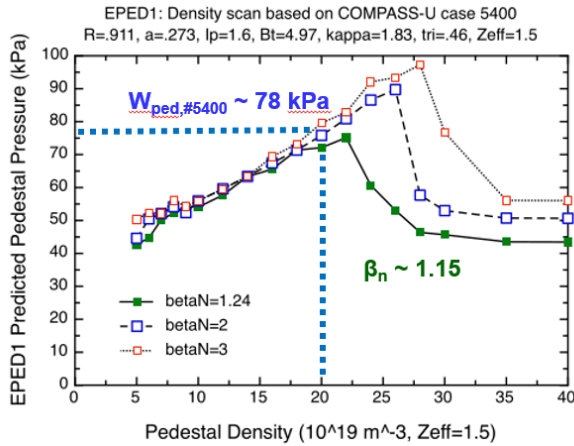
Validation of ELMy H-mode pedestal modelling with EPED

Transport simulations with METIS of ELMy H-mode use the scaling from [11] to estimate the pedestal top temperature:

$$T_{ped} = (0.025)^2 \left(\frac{1}{4\mu_0 e} \left(\frac{B_T}{q_{95}^2} \right)^2 \left(\frac{R}{a} \right)^2 \left(\frac{\alpha_c^2}{n_{ped}} \right) \left(\frac{\pi(1 + \kappa_{95}) q_{cyl}}{5 q_{95}} \right)^2 \right) \quad \alpha_c = 0.4s(1 + \kappa_{95}^2(1 + 5\delta_{95}^2))$$

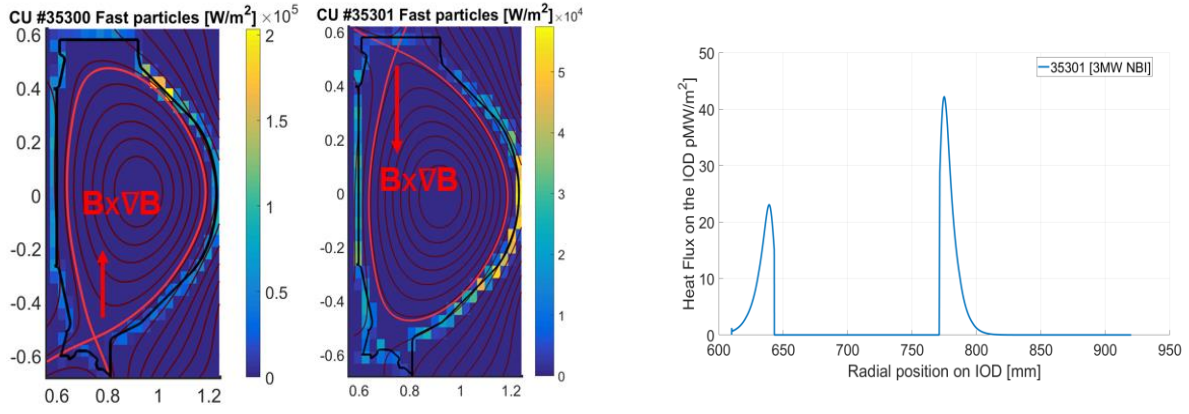
$$q_{cyl} = 5 \frac{a^2 B_t}{I_p \mu_0 R}$$

Comparison with EPED modelling shows that this is an upper estimate:



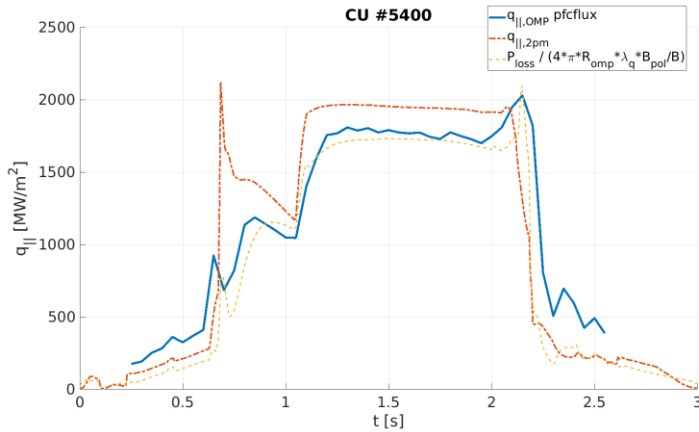
I-mode accessibility

I-mode experiments use the unfavourable drift configuration (ion ∇B drift away from the X-point), so that $P_{L,H,ELMy}$ is increased by a factor 2. I-mode can then be sustained at moderate heating power and lower collisionality. In the LSN configuration (#35300), the NBI will be injected in the counter-current direction and fast particles losses on the PFCs will be large.



Fast ions and fast neutrals losses for two possible I-mode configurations. The deposition and additional losses due to the Toroidal Field Ripple (TFR) and the Charge-Exchange (CX) with edge neutrals are given by the EBdyna code [15]. The heat flux on the Open Divertor in the USN configuration is large, making only a brief full-power I-mode possible in the clockwise field and current configuration (#35301): this could however be used as a way to enter Super H-mode [16].

Parallel Heat Flux on the PFCs and separatrix conditions



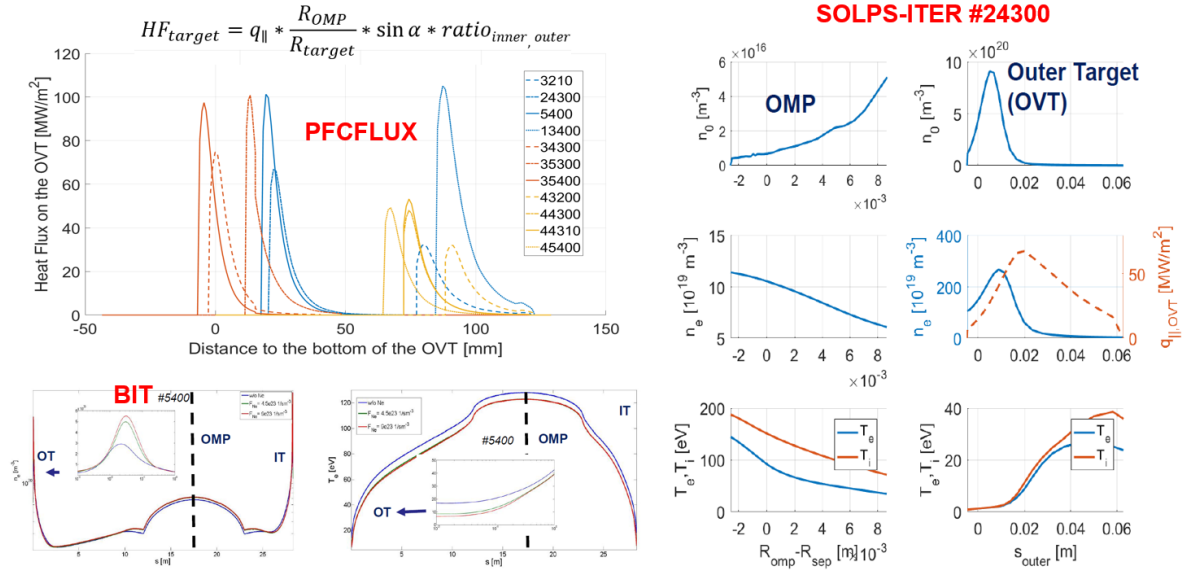
SOL conditions influence the separatrix conditions. In particular, the sheath-limited 2-point model [11] can be simplified to yield:

$$q_{||} = \frac{1}{2} \gamma_{\text{sheath}} n_e \frac{T_e + T_i}{2} \sqrt{2T_e/m_i}$$

Combining the knowledge of the parallel heat flux on the

target in the non-dissipative attached case as obtained from PFCFLUX [12] (with Brunner formula [13] and scaling [14] in H-mode) and the physics knowledge from the 2-point model [11], one can infer constraints on density and temperature at the LCFS (see table). For some scenarios, the 2-point model of METIS is necessary to recover the PFCFLUX heat flux.

Scenario	qp11_2pm [MW/m ²]	PCFLUX_q [MW/m ²]	METIS_q [MW/m ²]	ne_LCFS [10 ²⁰ m ⁻³]	Te_LCFS [eV]	Ti_LCFS [eV]	V _{e,SOL}
#24300	1475	1267	1258	1.18	132	176	7.7
#5400	1950	1862	1781	1.37	142	196	1.1
#35300	1012	1729	1898	0.32	215	397	0.8
#35400	1076	1925	2243	0.27	244	479	0.5
#44310	2184	1074	623.8	1.89	119	181	17.8
#45400	1874	1025	1296	1.89	115	146	16.4



The heat flux footprint predicted by the geometric model from PFCFLUX [12] differs significantly from the one calculated by the SOLPS-ITER (represented in the right figure for scenario #24300) fluid model or the BIT [17] PIC code indicating the likelihood of a large radiated fraction (46% for #5400 in BIT simulation) or quasi-detached plasma (SOLPS).

Conclusions and outlook

Transport modelling of various confinement regimes in the upcoming COMPASS Upgrade tokamak was performed with the fast transport solver METIS. We anticipate the pedestal conditions in various edge transport barrier MHD activities. SOL modelling allows to improve the modelling of separatrix conditions by the transport solver.

Acknowledgement

This work has been carried out within the framework of the project COMPASS-U: Tokamak for cutting-edge fusion research (No. CZ.02.1.01/0.0/0.0/0.0/16_019/0000768) and co-funded from European structural and investment funds. This work was supported by The Ministry of Education, Youth and Sports from the Large Infrastructures for Research, Experimental Development and Innovations project „IT4Innovations National Supercomputing Center – LM2015070“.

References

- [1] P. Vondracek et al. Fusion Eng. and Design 169 (2021) 112490
- [2] A.E. Hubbard et al 2017 Nucl. Fusion 57 126039
- [3] F. Ryter et al. 2014 Nucl. Fusion 54 083003
- [4] Y R Martin et al 2008 J. Phys.: Conf. Ser. 123 012033
- [5] W. Fundamenski et al 2012 Nucl. Fusion 52 062003
- [6] J. W. Hughes et al. (2002), Physics of Plasmas, 9(7):3019–3030
- [7] E.A. Tolman et al 2018 Nucl. Fusion 58 046004
- [8] T.M. Wilks et al 2019 Nucl. Fusion 59 126023
- [9] J.F. Artaud et al 2018 Nucl. Fusion 58 105001
- [10] T. Onjun et al., Physics of Plasmas 9, 5018 (2002)
- [11] Stangeby, Plasma Phys. Control. Fusion 60 (2018) 044022
- [12] J. Gerardin et al., Nucl. Mat. and Energy, 20, 2019, 100568
- [13] T. Eich et al 2011 Phys. Rev. Lett. 107 215001
- [14] D. Brunner et al 2018 Nucl. Fusion 58 094002
- [15] F. Jaulmes et al 2021 Nucl. Fusion 61 046012
- [16] P.B. Snyder et al 2015 Nucl. Fusion 55 083026
- [17] D. Tskhakaya et al., 25th Int. Conf. PSI in Contr. Fusion Devices